Molecular Dynamics of Monomeric Water Dissolved in Very Hydrophobic Solvents: the Current State of the Art of Vibrational Spectroscopy Analyzed from Analytical Model and MD Simulations

Y. Danten, T. Tassaing, and M. Besnard*

Laboratoire de Physico-Chimie Moléculaire (U.M.R C.N.R.S 5803), Université Bordeaux I, 351, Cours de la Libération, 33405 Talence, France

Received: March 22, 2000; In Final Form: June 26, 2000

The aim of the present paper is to evaluate the influence of the solute−solvent interactions on the infrared spectra of water diluted in liquid CCl_4 and in supercritical xenon, considered as the standard 'inert' solvent. This investigation is based upon FTIR spectra analyzed at the light of both analytical treatments and molecular dynamics simulations. For water in supercritical xenon, the rotational relaxation processes mainly determine the shape of the IR profiles associated with the ν_1 and ν_3 stretching modes. The water molecule rotates almost "freely" due to the isotropic character of the van der Waals interactions applied on the solute. Both the J-model for asymmetric molecular rotor and the molecular dynamics simulations properly account for the band shapes associated with the ν_3 and ν_1 vibrational modes of water. Thus, the rotational dynamics of water is primarily governed by "collisional" interactions with the neighboring solvent molecules. For water dissolved in liquid CCl_4, a structural analysis based upon the simulated radial distribution functions provides evidence for the existence of a short-ranged C···H−O arrangement between the solute and its neighboring solvent molecules. It is also found that the reorientational dynamics of water are more perturbed than those in SC xenon fluid, due to the weakly anisotropic character of the water-CCl_4 interactions. In particular, the reorientational motions of the z symmetry axis of water appear to be more specifically affected. We emphasize that a correct treatment of the rotational dynamics of water in liquid CCl_4 is provided only by simulation methods that, in contrast to the analytical J model, include the details of the intermolecular solute−solvent potential. Although the transition dipole moment of the ν_3 mode of water is only weakly affected by the interactions, the oscillator strength of the ν_1 internal mode is found to be enhanced compared to its gas-phase value, a result related to the increase of the transition dipole moment due to the water−solvent interactions. Finally, we argue that the spectral properties can be interpreted without invoking a specific H-bond contribution in the intermolecular potential.

I Introduction

The study of water extremely diluted in highly hydrophobic solvents has been a well-known research field in vibrational spectroscopy since the early 1960s.[1−8] These pioneering studies were aimed at understanding the spectral variations on going from the isolated molecule in gaseous phase to the dense phase, where the molecules experience many body interactions. The final objective was to obtain information at a microscopic level about the nature and the time scale of the main interaction processes. These two major achievements were only possible due to the very high sensitivity of infrared absorption spectroscopy, which is able to probe monomeric water in the liquid state. From these times, it has been well established that the fine rovibronic structure of the infrared spectra of isolated water is lost on going to states of higher densities. This conclusion has been inferred from a large body of studies that have been mostly concerned with the symmetric ν_1 and anti-symmetric ν_3 stretching vibrations of water and to a much lower extent with the ν_2 bending mode. We recall that for water, which is an asymmetric top molecule, the stretching vibrations give rise in the gas phase to a very complicated fine structure resulting from the two rovibronic spectra respectively centered at about 3657 and 3756 cm^{-1} which greatly overlap.[9] Further experimental investigations on water diluted in series of organic solvents have revealed that the strength due to a "specific interaction" could be characterized by a redshift of the band center observed for the two stretching vibrations correlated with a blue shift of the ν_2 bending band. In this context, the liquid carbon tetrachloride (CCl_4) appeared to be the weakest interacting solvent. This is supported by a small redshift of the ν_1 and ν_3 internal modes of water (respectively at about 3613 and 3708 cm^{-1}) and the well-defined wing (at about 3800 cm^{-1}) associated with the antisymmetric ν_3 mode, interpreted as being the remnant of the rotational structure observed in gaseous state. Thus, it has been inferred that the rotational motion of water is only very slightly hindered in liquid CCl_4. In 1985, the vibrational spectra of water dissolved in liquid alkanes were reported for the first time by *Conrad and Strauss* in a study aimed at the understanding of very weak hydrogen bond signature in the context of a biological investigation.[10] In alkanes, only the ν_3 mode was observed, and the band shape of the associated spectrum exhibits sidebands, which have been described in terms of P and R branches, a terminology used for the rovibronic spectra observed in the gas phase. Using the Gordon J-model (vide-infra), it was subsequently established that monomeric water performs large angular variations in the meantime between collisions with the solvent molecules. Therefore, the existence of a specific interaction (namely hydrogen-bond) in the alkanes was ruled out. In

10.1021/jp001091p CCC: $19.00 © 2000 American Chemical Society
Published on Web 10/04/2000

contrast, for water dissolved in liquid CCl_4, higher redshifts on the ν_1 and ν_3 modes were observed.[11] Moreover, attempts to use the J-model to interpret the band shape of the ν_3 stretching mode of water failed. These findings led to the conclusion that water and CCl_4 form a very weak complex.

More recently, the rotational relaxation of D_2O dissolved in xenon has been studied at $T \approx 383$ K, as a function of the density using infrared absorption and molecular dynamics (MD) simulation.[12] The ν_3 mode of monomeric water was clearly observed and found to present very well defined P and R branches even at the highest densities investigated in supercritical (SC) xenon. These results, which are supported by an analysis of the experimental dipole autocorrelation using MD simulation, show that water rotates "freely" in this solvent. These findings led to the conclusion that xenon and the alkanes are solvents in which there is no specific interaction with water.

The study of water weakly interacting with solvents has more recently enjoyed an upsurge of interest. In this context, the existence (or nonexistence) of a very weak hydrogen bond in the water-benzene mixture has been thoroughly investigated.[13−20] A large number of experimental and theoretical investigations have addressed this question from the study of the isolated dimer observed in rare gas matrixes and supersonic cooled jet beams at low temperatures (in the temperature range of ∼5 to 10 K).[21−29] Similarly, in the liquid state, at room temperature and at high pressure and temperature, several spectroscopic studies have been also performed with the aim of detecting and characterizing the interaction between the molecules.[30−38] Convincing factual evidence, which gave support to the existence of a very weak hydrogen bond between water and benzene was obtained. Very recently, we have even proposed, from an ab initio and infrared study, rationalizing the interaction of water diluted in fluorinated benzenes in term of the more general Lewis acid−base concept solvent.[39] From all the investigations reported so far, it comes out that, at a qualitative level, water in liquid CCl_4 can be classified as a system intermediate between the water−xenon and water−alkanesystems and the water−benzene system. In the former, the water rotational motion is "quasi free", and a collisional picture is rather well adapted to characterize the molecular dynamics. In contrast, the rotational motion in benzene solution is more hindered, a fact ascribed to the existence of a very weak hydrogen bond.

The aim of the present article is to investigate the molecular dynamics of the water−tetrachloride system, for which only sparse information on the molecular dynamics is currently available. For this purpose, we present herein the analysis of the measurements that we have performed on water−CCl_4 system in the far- and mid-infrared spectral range analyzed at the light of a theoretical investigation based upon the use of both analytical model and molecular dynamics simulation. This paper comprises three main sections, outlined as follows:

In the first part, we review the basic spectroscopic theoretical background relevant for our study. In particular, we will present the pertinent literature results concerning the infrared (IR) spectra of water in gas phase and isolated in SC xenon. These elements are needed to understand the influence of the water−solvent interaction on the intensities and band shapes of the infrared (IR) profiles associated with the ν_1 and ν_3 stretching modes of water in the following. Indeed, as far we know, the origin of the activation of the ν_1 mode of water observed in liquid CCl_4 has surprisingly never been addressed in depth.

The second part will be devoted to the presentation of the IR absorption measurements of the ν_1 and ν_3 modes of water in liquid CCl_4 at room temperature. The spectra will be analyzed (shifts, intensities, and band-shapes) and compared with available literature studies. Then, the analytic treatment of the band shape, performed using the Gordon's J-model adapted for asymmetric top molecules (not previously reported at this level), will be applied and critically discussed.

In the third part, we will present the structural and dynamical properties obtained by MD simulation on water diluted in liquid CCl_4 at room temperature. The discussion of these results has been performed at the light of the MD simulation of the water/xenon mixture, considered here as the reference system in which the solvent is fully "inert". In particular, the rotational relaxation processes of light and heavy water around its main symmetry axes have been further analyzed to assess the influence of their contributions in the vibration−rotation spectra. Finally, on the basis of the results obtained in this study, the nature and time scale of the water−solvent interactions are discussed.

II Material Background on the Infrared Absorption of Monomer Water

In this section, we will present the basic theoretical background concerning infrared absorption spectroscopy. Then, we will put the emphasis on the pertinent facts obtained from the literature, those needed to introduce the problematic relative to water in a solitary state in a liquid "inert" solvent.

II-1 Theoretical Background. The linear absorption coefficient of a sample absorbing an electromagnetic radiation is related to the spectral density $I(\omega)$ by the following relationship[40]

$$\alpha(\omega) = \frac{4\pi^2}{3\hbar cV}\frac{1}{n}\left(\frac{n^2+2}{3}\right)\omega[1 - \exp(-\beta\hbar\omega)]I(\omega) \quad (1)$$

where, V is the volume of the sample, c is the velocity of the light, $\hbar$ is Planck's constant, $\beta = 1/k_BT$ (with k_B, the Boltzmann constant and T the temperature of the sample), and n is the refractive index, assumed to be frequency independent.

The spectral density $I(\omega)$ is the time-Fourier transform of the autocorrelation function (acf) $C(t)$ of the sample dipole moment $\vec{M}(t)$ according to

$$I(\omega) = \frac{1}{2\pi}\int_{-\infty}^{+\infty} dt\, e^{-i\omega t}\langle\vec{M}(t)\cdot\vec{M}(0)\rangle \quad (2)$$

For a solute that is highly diluted in a solvent, it is assumed that the interactions between vibrations belonging to two distinct solutes can be neglected. Moreover, if it is also assumed that the rotational and vibrational degrees of freedom are uncoupled and that induction processes (e.g., dipole induced dipole interactions) are absent, it can be shown that the spectral density $I(\omega)$ associated with a particular infrared transition is given by[41]

$$I(\omega) = \frac{N}{2\pi}\int_{-\infty}^{+\infty} dt\, e^{-i\omega t}\left(\frac{\partial\mu}{\partial q}\right)_{q_0}^2\langle\vec{u}(t)\cdot\vec{u}(0)\rangle\langle q(t)q(0)\rangle \quad (3)$$

where, $\vec{u}$ is the unit vector lying along the transition dipole moment $(\partial\mu/\partial q)_{q_0}$ associated with the normal coordinate q, and N is the number of solute molecules.

Therefore, the spectral density $I(\omega)$ results from the convolution of the spectral density $I_{rot}(\omega)$ due to the rotational motions of the solute molecule with the spectral density $I_{vib}(\omega)$ associated with the vibrational relaxation of the studied normal mode, i.e.,

$$I(\omega) = \left(\frac{\partial\mu}{\partial q}\right)_{q_0}^2\int_{-\infty}^{+\infty} d\omega' I_{rot}(\omega')I_{vib}(\omega-\omega') \quad (4)$$

with,

$$I_{\mathrm{rot}}(\omega) = \int_{-\infty}^{+\infty} dt\, e^{-i\omega t} \langle \vec{u}(t) \cdot \vec{u}(0) \rangle \tag{5}$$

and

$$I_{\mathrm{vib}}(\omega) = \int_{-\infty}^{+\infty} dt\, e^{-i\omega t} \langle q(t) q(0) \rangle \tag{6}$$

This approach applied to the fundamental transitions ν_1, ν_2, and ν_3 of monomeric water leads to the following autocorrelation functions (acf):[42]

$$\begin{cases} C^{V}{}_{1}(t) = N\left(\dfrac{\partial \mu}{\partial q_1}\right)^2 \langle \vec{u}_z(0) \cdot \vec{u}_z(t) \rangle \langle q_1(0)\, q_1(t) \rangle \\ C^{V}{}_{2}(t) = N\left(\dfrac{\partial \mu}{\partial q_1}\right)^2 \langle \vec{u}_z(0) \cdot \vec{u}_z(t) \rangle \langle q_2(0)\, q_2(t) \rangle \\ C^{V}{}_{3}(t) = N\left(\dfrac{\partial \mu}{\partial q_1}\right)^2 \langle \vec{u}_y(0) \cdot \vec{u}_y(t) \rangle \langle q_3(0)\, q_3(t) \rangle \end{cases} \tag{7}$$

It appears from these expressions that the IR absorption profiles associated with the bending ν_2 mode and the symmetric stretching ν_1 mode of water provide information on the reorientational motions of the unit vector u_z (B-type band) lying along the C_2-symmetry axis. Whereas, the antisymmetric stretching vibration ν_3 of water gives access to the reorientational motions of the unit vector u_y lying in the plane of the molecule and perpendicular to the C_2 axis (A-type band). Finally, we notice that the reorientational motions of the unit vector u_x out of the molecular plane (C-type band) is not involved in the observed IR absorption profiles of water.

II-2 Background Literature Elements on the Infrared Spectra of Water in Gas Phase and Isolated in Supercritical Xenon. The mid infrared (MIR) spectrum of water in gaseous phase is well-known and has been extensively studied.[9] In Figure 1, we have reported the experimentally observed spectrum of the ν_1 and ν_3 stretching vibrational modes (see the inset), which exhibits a complicated overlapping rovibronic structure. The measured vibrational intensities obtained from the sum of all of the observed rotational transitions assigned to the separate of the vibrational transition ν_3 and ν_1 lead to a ratio of about 15,[14] which shows that the ν_3 transition is by far the most intense in the gas phase. In contrast, in dense phases, due to the "collisions" experienced by the water molecule with the solvent, the quantum rotational fine structure of the spectrum collapses and leads to a continuous envelop. If the meantime between collisions is much greater than the period of free rotation of water, the spectrum can be calculated in the framework of classical mechanics. In this context, the rotational profile calculated for water, which is an asymmetric top molecule of C_{2v} symmetry, leads to a ν_1 band, which presents a P, R structure (B-type band), whereas the ν_3 band exhibits a P, Q, R stucture (A-type band). This observation is perfectly illustrated in the case of water dissolved in xenon as a function of increasing pressure at constant temperature.[12] At the highest density investigated, the spectrum of water in supercritical xenon exhibits the rotational P and R branches, flanking the central Q-branch associated with the ν_3 transition (Figure 1). Moreover, if we consider the relative intensities of the two stretching vibrations of water measured in the gas phase, it seems that the ν_1 contribution in the spectrum can be safely neglected. However, a closer examination of Figure 1 shows that the intensity of the P branch is slightly greater than the R one. This result is in contradiction with the ratio of the intensity of the rotational branches, which is governed by the Maxwell−Boltzmann distribution, namely, the detailed balance principle.[43] It might be inferred from this observation that the contribution of the ν_1 mode from the gas-phase result is much greater than expected. This point, which is not reported by these authors,[12] will be discussed below.

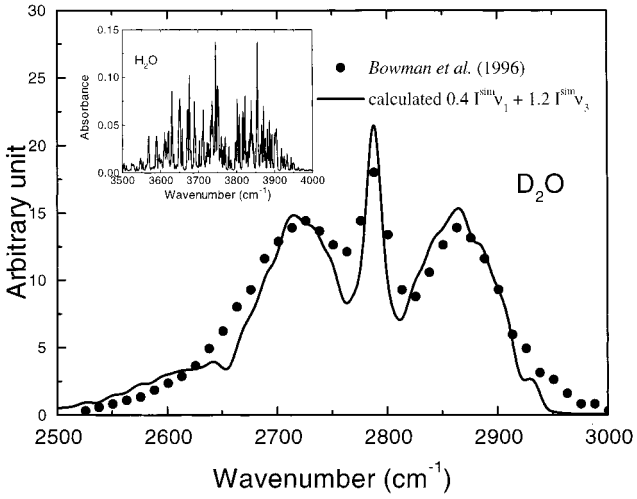

Figure 1. Experimental infrared spectrum of the ν_3 anti-symmetric stretching mode of heavy water (D_2O) in supercritical xenon fluid (filled circles) ($T = 383$ K, $\rho = 15.6 \times 10^{-3}$ mol/cm^3).[12] We have displayed the weighted sum of the type A (for the ν_1 mode) and type B (for the ν_3 mode) simulated rotational profiles of D_2O in solid line. For illustration, we have also reported in the inset the fine overlapping rovibronic structure of light water (H_2O) in gaseous phase.

III Infrared Absorption Spectra of Water Dissolved in Liquid CCl_4

III-1 Experimental Details. The solutions were prepared by mixing ultrapure water (milli Q, 18 MΩ) with carbon tetrachloride (Aldrich, purity +99%), dehydrated for several days on molecular sieves. We have carefully checked to ensure that the solutions were properly equilibrated by making several measurements during the several days after mixing. In addition, we know from our previous infrared spectroscopic works that water oligomers do not contribute to our spectra.[15] The reproducibility of the measurements indicates that the solutions were saturated in water, and we assumed that the concentration was 8.4 10^{-4} in molar fraction at room temperature (∼25 °C) as reported from thermodynamic measurements in the literature.[44]

The mid-infrared spectra have been recorded on a Bio-Rad interferometer by accumulating 100 spectra recorded at 2 cm^{-1} spectral resolution. The ν_3 and ν_1 modes as well as the $\nu_2 + \nu_3$ combination of water have been recorded. The observation of the ν_2 bending vibration was hampered by the strong contribution of the internal modes of the solvent. The cell that was used was made with CaF_2 windows and had a 3 cm path length.

III-2 Experimental Observations. The spectra of water diluted in CCl_4 corrected from the solvent contribution are reported for the ν_1 and ν_3 fundamental transitions and for the $\nu_2 + \nu_3$ combination in Figure 2. The profiles associated with the two stretching vibrations display the general features that have been previously reported in earlier studies, namely two well-defined peaks corresponding to the ν_1 and ν_3 modes and remnant rotational wings clearly apparent on the profile associated with the ν_3 mode. If we consider the spectra associated with the combination mode, we find that its band shape is almost identical to the band shape of the ν_3 mode (vide-infra). It is noteworthy that the $\nu_2+\nu_1$ combination mode, although spectrally allowed by group theory (both vibrations belong to the

TABLE 1: Spectroscopic Data for Water Diluted in Liquid CCl_4 at Room Temperature[a]

ν_1 stretching mode			ν_3 stretching mode					$\nu_3 + \nu_2$ combination mode			
ν_1 (cm^{-1})	η_1 (Nep. cm^{-2})	$\Delta\nu_1$ (cm^{-1})	ν_3 (cm^{-1})	η_3 (Nep. cm^{-2})	$\Delta\nu_3$ (cm^{-1})	η_3/η_1	ref	$\nu_3 + \nu_2$ (cm^{-1})	η (Nep. cm^{-2})	$\Delta\nu$ (cm^{-1})	ref
3613.0			3708.0				[4−6] 25 °C				
3619.0			3710.0		39.0		[8] 30 °C	5283.0		39.0	[8]
3613.0	13 [£][b]	38.0	3705.0	34[£]	42.0	2.6	[7] (30 °C)	5282.0		37.0	[11]
3617.0		15.0	3708.0		31.0		[11] 25 °C	5285.0	2.5	40.0	our work
3616.0	10	19.0	3709.0	34.5	37.0	3.45	our work				
3657.1	2.97		3755.9	43.2			gas phase [9]				

[a] Band center frequencies (ν), integrated intensities (η) and full widths at half-height ($\Delta\nu$). [b] [£] Intensity measured at the maximum of the band (in l mol^{-1} cm^{-1} unit).

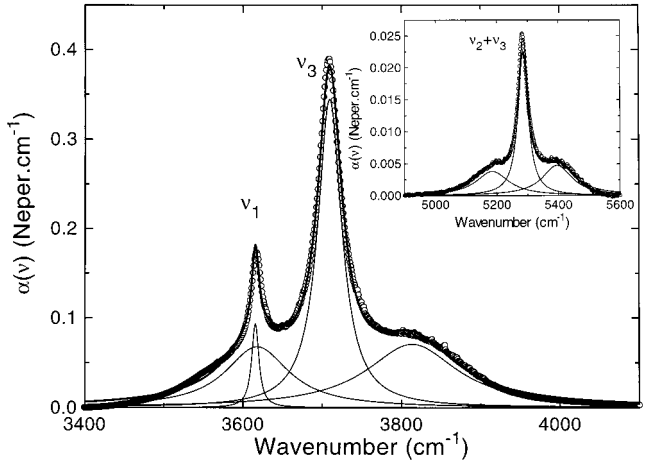

Figure 2. Experimental infrared spectrum of the ν_1 and ν_3 stretching vibrational modes of water diluted in liquid CCl_4 at room temperature (circles). We have also reported the measured absorption profile associated with the $\nu_2 + \nu_3$ combination mode of water (circles) in the inset. The Lorentzian band shape decomposition of the profiles is indicated by the thin solid lines on each figure.

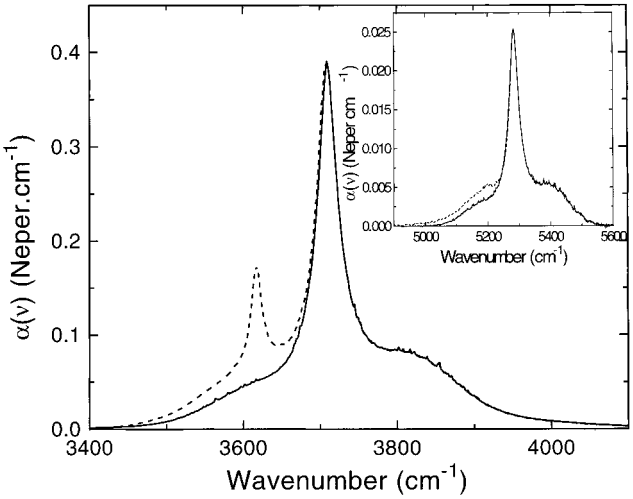

Figure 3. Contribution of the ν_3 vibrational mode (solid line) on the infrared spectrum due to the fundamental transitions of water in liquid CCl_4 (dashed-line), which has been evaluated from the symmetrization procedure used in our study (see text). We have also reported in the inset the same band shape analysis for the profile associated with $\nu_2 + \nu_3$ combination mode.

A_1 representation, which is infrared active) is not clearly observed in this spectral range.

We have checked the quality of our measurements by comparing them with the literature data (see Table 1). For this purpose, we have performed a simple quantitative analysis of the band shape reported in Figure 2, using Lorentzian profiles to evaluate the position of the band center, the fullwidth of the central branch and the ratio of the integrated intensities (I_{ν_3}/I_{ν_1}) of the ν_1 and ν_3 bands. The fitted values are reported in comparison with literature available data in the Table 1. From this comparison, it appears that there is an overall fair agreement between the band center and the fullwidth reported in earlier studies with our measurements. However, the quality of our data allows to discuss more accurately the band shapes of the ν_1 and ν_3 profiles and, in particular, to extract their respective integrated intensities. Indeed, up till now, have been reported in the literature the values of the extinction coefficient ϵ_{max} taken from the maxima of the ν_1 and ν_3 profiles. To have an accurate determination of the integrated intensities, we have to separate the contribution of the ν_1 mode, which overlaps strongly with the ν_3 band. Thus, we have assumed that the high-frequency wing of the ν_3 mode is not affected by the contribution of ν_1 mode.

In consequence, we have obtained the low-frequency part of the ν_3 profile from its high-frequency side as follows. In a first step, we have calculated using eq 1 the spectral density $I(\omega_0 + \Delta\omega)$ associated with the high-frequency side (where ω_0 is the band center frequency, and the frequency deviation from it is $\Delta\omega = |\omega - \omega_0|$. Then, we have applied the detailed balance relationship that relates the intensity of the low and high-frequency parts of the profile, i.e.,

$$I(\omega_0 - \Delta\omega) = I(\omega_0 + \Delta\omega) \exp(-\beta\hbar\Delta\omega) \qquad (8)$$

Finally, the absorption coefficient associated with the low-frequency side has been obtained by applying the eq 1 to $I(\omega_0 - \Delta\omega)$. More succinctly, the upper and lower parts of the ν_3 profile are related by

$$\alpha(\omega_0 - \Delta\omega) = \left[\frac{\omega_0 - \Delta\omega}{\omega_0 + \Delta\omega} \cdot \frac{1 - e^{-\beta\hbar(\omega 0 - \Delta\omega)}}{1 - e^{-\beta\hbar(\omega 0 + \Delta\omega)}}\right] e^{-\beta\hbar\Delta\omega} \alpha(\omega_0 + \Delta\omega) \qquad (9)$$

The resulting profile, which is presented in Figure 3, is the determination of the profile of the ν_1 mode by subtraction. The integrated intensities of the ν_3 and the ν_1 mode evaluated with a relative error estimated respectively as 10% and 40% are reported in Table 1. From these values, we can calculate the oscillator strength f of the vibrational transition. We have obtained a value of $(7.4 \pm 0.8)\ 10^{-6}$ for the ν_3 mode and $(2.2 \pm 0.9)\ 10^{-6}$ for the ν_1 mode, which can be compared with the corresponding values for water in the gaseous phase, which are $8.3\ 10^{-6}$ and $5.6\ 10^{-7}$, respectively.[15] Within experimental uncertainties, the oscillator strength of the ν_3 mode measured in the water/CCl_4 solution remains close to its gas-phase value, whereas there is a sizable enhancement of the oscillator strength of the ν_1 mode. We have also performed the detailed balance numerical treatment on the profile associated with the $\nu_2 + \nu_3$

combination band (inset Figure 3). The resulting profile is compared with the experimental one. A small excess of intensity is observed on the low-frequency side of the $\nu_2 + \nu_3$ combination band, which can be assigned to the $\nu_1 + \nu_3$ combination band. If this assignment is correct, it appears that the band shapes associated with the ν_1 mode and the combination $\nu_1 + \nu_3$ are different. This finding is in contrast with the similarity observed between the band shapes of the ν_3 and the $\nu_2 + \nu_3$ profiles. The integrated intensities of the combination of the ν_3 and the ν_1 mode evaluated with a relative error estimated respectively as 20% and 60% are reported in Table 1. Therefore, the oscillator strength can be calculated, and we have obtained a value of $(5.4 \pm 1.2)\ 10^{-7}$ for the $\nu_2 + \nu_3$ mode and a value of $(5 \pm 3)\ 10^{-8}$ for the $\nu_1 + \nu_3$ mode, which can be compared with the corresponding values for water in the gaseous phase, which are 9.10^{-7} and $4.2\ 10^{-8}$, respectively.[14] In view of experimental uncertainties, we can assume that the oscillator strengths of the combination bands of water in CCl_4 solution are the same than those reported for the gas phase.

III-3 Interpretation of the Band Shapes using an Analytical Model. It is noteworthy from the presentation of the experimental results reported for water dissolved in xenon, which is undoubtedly the more "inert" solvent, that the rotational dynamics plays a major role in conditioning the band shape.[12] Similarly, the presence of well-defined rotational wings in the profile associated with the ν_3 mode of water in liquid CCl_4 also supports this viewpoint. In this context, we have tried to use the analytical J diffusion model to fit our data. In this model, water is considered to be an asymmetric top molecule performing free rotational periods governed by the three main inertial moments, which are interrupted by collisions with the solvent molecules. The instantaneous binary isolated collisions are assumed to obey a Poisson's distribution.[45,46] After each collision, the orientation of the angular momentum is randomized, and its magnitude is redistributed according to the Maxwell−Boltzmann distribution law. The main advantage of this model is to use a single adjustable parameter, namely τ_J^*, the meantime between collisions (the correlation time of the angular momentum) to treat the rotational dynamics. Using reduced units, we can define τ_J^* as

$$\tau_j^* = \sqrt{\frac{kT}{I_B}}\tau_j \qquad (10)$$

where, I_B is the inertial moment along the Y axis (in the molecular plane and perpendicular to the C_2 symmetry axis).

Two limiting cases are recovered, namely the "free" rotation limit where $\tau_J^* \gg 1$ and the rotational diffusion where $\tau_J^* \ll 1$. In the "free" rotation limit ($\tau_J^* \gg 1$), the rotational profile of the A-type band exhibits a well-defined PQR-structure. When the molecule experiences collisions ($\tau_J^* \approx 1-2$), the Q-branch broadens and its intensity decreases, whereas the rotational wings on both sides of this central peak become less pronounced. Finally, a single Lorentzian profile is observed as the diffusive rotational regime is reached ($\tau_J^* \ll 1$). In the case of the B-type band, the profile presents a P−R structure characterized by the presence of a central dip, which is progressively filled up when the frequency of the collisions with the solvent molecules increase. As before, in the diffusive rotational regime, the profile becomes again of the Lorentzian type.

We have used the analytical J model to calculate the spectral densities for the ν_3 mode (A type band) and the ν_1 mode (B type mode) of light water at temperature about 300 K as a function of τ_J^* (Figure 4). This model is able to retrieve the

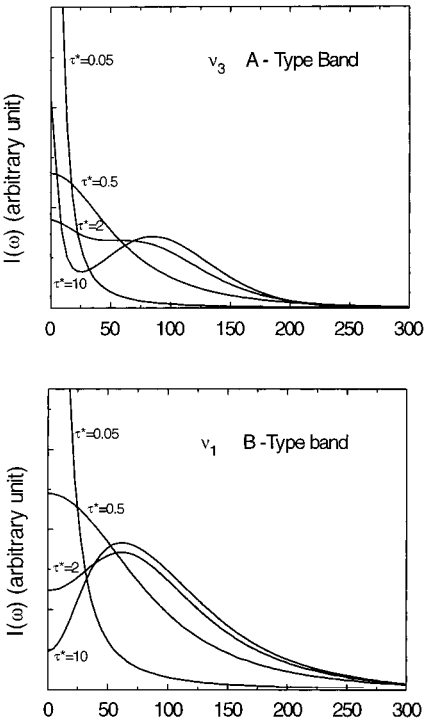

Figure 4. Calculated spectral densities of light water (H_2O) using the J model for the ν_3 mode (A type band) and the ν_1 mode (B type mode) for different values of τ_J^* and a temperature of about 300 K.

evolution of the experimental band shapes including the wings observed on the ν_3 band as well as the behavior of the PR structure of the ν_1 mode existing in the gas phase and which is collapsed toward a Lorentzian profile under the influence of the intermolecular collisions. However, this is only possible by using a different correlation time of the angular momentum for each mode, $\tau_J^* \approx 10$ and $\tau_J^* \approx 0.05$, respectively, for the ν_3 and ν_1 modes. Although, extended J models using two collision times have been proposed, the main drawbacks of the model still reside first in the neglect of the attractive part of the interaction potential and second in the assumption of the instantaneous duration of the collisions. Thus, treatments aimed at the characterization of the nature of the solute−solvent interaction of water in liquid CCl_4 and which are based on the study of rotational dynamics using the J model even in its more sophisticated version (for asymmetric top molecules) are questionable. Due to the limitation of this model, the conclusions concerning the rotational dynamics are indeed dependent upon the choice of the normal mode investigated. Thus, the absence of viable analytical treatment prompted us to rely on a molecular dynamics simulation for interpretative purposes.

IV Molecular Dynamics Simulation

IV-1 The Modeling of the Water−Solvent Interaction Potential. This section is devoted to the discussion of a semiempirical model of the intermolecular interactions to study by molecular dynamics simulations the structural and dynamical properties of mixtures of water dissolved in liquid CCl_4 and in supercritical (SC) xenon fluid.

In these simulations, the molecules are treated as rigid units. The modeling of the intermolecular interactions is based on the use of an isotropic atom−atom potential, which is decomposed in a sum of repulsive and dispersive terms. Moreover, we have explicitly included in the potential energy model, the electrostatic interaction contributions by placing point charges on the atoms of the water and CCl_4 molecules.

TABLE 2: Interatomic Potential Parameters for the CCl_4-CCl_4 and H_2O-CCl_4 Interactions and Molecular Point Charge Distributions[a]

interatomic {exp-6} potential parameters for the CCl_4-CCl_4 interactions	$B_{\alpha\beta}$ (kJ/mol)	$C_{\alpha\beta}$ ($Å^{-1}$)	$A_{\alpha\beta}$ (kJ $Å^6$/mol)
C−C	1.23×10^6	2.971	13 370.0
Cl−Cl	3.05×10^6	3.970	5134.9
interatomic LJ potential parameters for the H_2O-CCl_4 interactions	$\epsilon_{\alpha\beta}$ (kJ/mol)		$\sigma_{\alpha\beta}$ (Å)
O−O	0.651		3.165
Cl−Cl	0.851		3.500
C−C	0.425		4.600
	atomic point charge| distribution (in electron unit)		
CCl_4 molecule	$q_{cl} \approx +0.2920$		$q_c \approx -1.1680$
H_2O molecule	$q_H \approx +0.3356$		$q_o \approx -0.6712$

[a] The cross atom−atom potential parameters are obtained from the usual combination Lorentz−Berthelot rules.

For the nonflexible model used here, the structure of the CCl_4 molecules is fixed at the experimental tetrahedron (Td) geometry with a C−Cl bond length of 1.769 Å.[47] The atomic charge distribution on the CCl_4 molecules was determined in order to reproduce the experimental value of the octopole moment in liquid phase ($\Omega \approx 14.96\ 10^{-34}$ esu)[48,49] (cf. Table 2).

For the modeling of the CCl_4-CCl_4 intermolecular interactions, we have chosen to use an isotropic atom−atom potential using an analytical form of type {exp-6-1} given by

$$U_{\alpha\beta}(r_{\alpha\beta}) = B_{\alpha\beta}\exp(C_{\alpha\beta}r_{\alpha\beta}) - \frac{A_{\alpha\beta}}{r_{\alpha\beta}^{\,6}} + \frac{q_\alpha q_\beta}{r_{\alpha\beta}} \qquad (11)$$

where α and β label the C, Cl, O, and H atoms, respectively, and $r_{\alpha\beta}$ is the distance between the atoms α and β belonging to two interacting molecules.

This potential model has been used for the neat liquid CCl_4 and for the water/CCl_4 solution and the atom−atom potential parameters (B, C, and A) used here are reported in Table 2.

The rigid molecular geometry of water is defined as in the *Berendsen's* SPC model.[50] For water diluted in a nonpolar solvent, the dipole moment is expected to be close to the gas value ($\mu \approx 1.87$ D) and therefore, the atomic charges used were fixed in order to reproduce the latter one. The values of the point charges for water and carbon tetrachloride used in our calculations are also reported in Table 2.

The H_2O-CCl_4 interaction potential is modeled from an analytic expression of the Lennard−Jones type according to

$$U_{\alpha\beta}(r_{\alpha\beta}) = 4\epsilon_{\alpha\beta}\left(\left(\frac{\sigma_{\alpha\beta}}{r_{\alpha\beta}}\right)^{12} - \left(\frac{\sigma_{\alpha\beta}}{r_{\alpha\beta}}\right)^{6}\right) + \frac{q_\alpha q_\beta}{r_{\alpha\beta}} \qquad (12)$$

The LJ atom−atom parameters ϵ and σ describing the intermolecular interactions were obtained from the potential models proposed by Mc Donald for CCl_4[49] and by Berendsen (SPC model) for water.[50] Finally, the cross parameters of the water−CCl_4 potential have been obtained according to the usual Lorentz−Berthelot mixing rules. Then, the electrostatic part of the intermolecular potential is completely defined from the atomic charge distributions of the H_2O and CCl_4 molecules. Clearly, in the limit of the highly diluted solutions considered here, the electrostatic terms are aimed to reproduce the dipole−octopole and octopole−octopole contributions for the respective H_2O-CCl_4 and CCl_4-CCl_4 interactions. All of the potential parameters used in our simulations are reported in Table 2.

TABLE 3: Interatomic LJ Potential Parameters for the H_2O-Xe and Xe−Xe Interactions

LJ potential parameters in the H_2O-Xe system	$\epsilon_{\alpha\beta}$ (kJ/mol)	$\sigma_{\alpha\beta}$ (Å)
Xe−Xe	1.837	4.100
Xe−O	1.083	3.633

For our study of water in SC xenon fluid, we have used the model originally proposed by Mc Donald and Singer to describe the interatomic Xe−Xe forces.[51] We have applied the previous approach in order to define the Xe−H_2O interactions using an analytical expression of Lennard−Jones type. The LJ atom−atom potential parameters ϵ_{ij} and σ_{ij} used in the simulation are reported in Table 3.

IV-2 Computational Details. We have performed a molecular dynamics simulation of nonflexible molecules in the microcanonical ensemble (N, V, E). The sample was composed of a single H_2O (or D_2O) molecule and 107 CCl_4 solvent molecules confined in a cubic cell of constant volume. Using the periodic boundary conditions, the equations of motion were solved by a leapfrog algorithm with a time step of 0.5×10^{-15} s to ensure a good conservation of the total mechanical energy of the system during the MD run. The molecular rotations were treated in the framework of the quaternions formalism. The cutoff radius of the intermolecular forces was equal to half the box length L, whereas long-range corrections corresponding to the repulsive and the dispersive part of the potential were added to the pressure and the internal energy. The calculations were performed at a temperature of 300 K for a molar density number of the sample $\rho \approx 10.3 \times 10^{-3}$ mol/cm^3 (or a molar volume $V_m \approx 97.36$ cm^3/mol) and a production run of 600 ps after an equilibration time of 75 ps was recorded for the needs of our study. For the sake of comparison, we have also performed a simulation of the neat liquid CCl_4 in the same thermodynamic conditions as previously recorded but with a simulated sample composed of 256 molecules in the cubic cell and the use of a satisfactory time step of 10^{-14} s required for the integration of the molecular trajectories. Here again, a production run of 600 ps was carried out (or 60 000 run steps) after an equilibration time of 75 ps.

For the purpose of our discussion, we have also performed several simulations under the same overall computational conditions on a mixture composed of a single water molecule (H_2O and D_2O as well) dissolved in a solvent constituted of 255 xenon atoms. The runs were performed during 600 ps after 188 ps of equilibration. The temperature and density of xenon were respectively chosen at $T \approx 383.15$ K and $\rho \approx 15.6\ 10^{-3}$ mol/cm^3. It is under these specific thermodynamics conditions that the experimental infrared spectra in the region of the stretching vibration exhibits, as we have discussed previously, a profile comprising the envelopes of the rotational P and R transitions. We will show in the following that the choice of these density conditions is the most convenient for a comparison with the spectra of water dissolved in CCl_4 at room temperature.

IV-3 -A Structural properties. IV-3 Molecular Dynamics Results. The calculated thermodynamic properties for hydrogenated (H_2O) and deuterated (D_2O) water diluted in liquid CCl_4 at room temperature and for D_2O dissolved in SC xenon fluid at the temperature $T = 383.15$ K are listed in Table 4 and are compared with those corresponding to the pure solvents simulated in the same thermodynamic conditions. Notice that the value of the mean intermolecular potential energy obtained for the pure liquid CCl_4 is in good agreement with the values

TABLE 4: Simulated Thermodynamic Properties for the H_2O/CCl_4 and D_2O/CCl_4 Solutions at Room Temperature ($\rho \approx 10.3\ 10^{-3}$ mol/cm^3) and for D_2O Dissolved in the Supercritical Fluid Xenon ($T \approx 383$. K and $\rho \approx 15.6\ 10^{-3}$ mol/cm^3)[a]

simulated systems	potential energy U_p (kcal/mol)	T (K)	$\lvert\Delta E_T\rvert/\lvert E_T\rvert$
H_2O/CCl_4	-7.23 ± 0.06	282.2	1.0×10^{-4}
D_2O/CCl_4	-7.17 ± 0.06	292.7	1.4×10^{-4}
neat CCl_4 liquid	-7.27 ± 0.04	300.8	7.2×10^{-4}
D_2O/SC xenon	-1.80 ± 0.03	390.4	$\sim 5 \times 10^{-4}$
pure SC xenon	-1.82 ± 0.03	385.2	$\sim 1.5 \times 10^{-4}$

[a] For a studied system, $\Delta E_T/E_T$ represents the relative deviation of the total energy cumulated on the total simulation time.

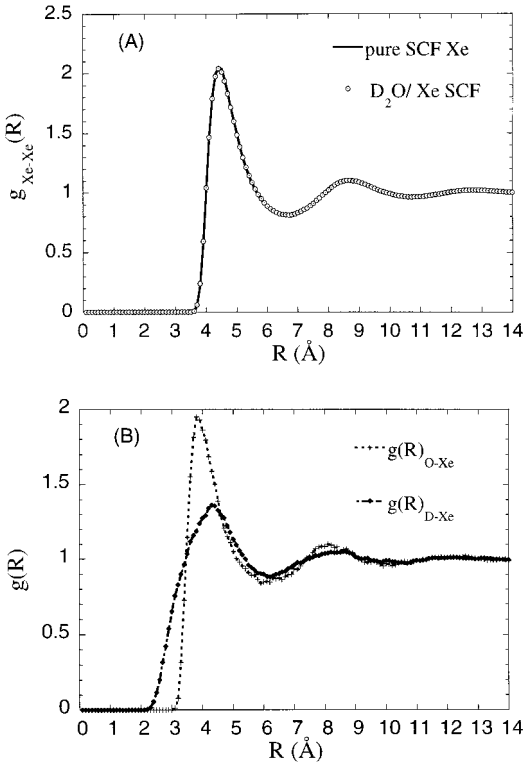

Figure 5. Simulated radial distribution functions (rdf) for the SC mixture D_2O/xenon ($T \approx 383.15$ K and $\rho \approx 15.6 \times 10^{-3}$ mol/cm^3). (a) the rdf $g_{Xe-Xe}(r)$ calculated in the mixture D_2O/xenon and compared with the one in the pure SC xenon; (b) the rdf $g_{O-Xe}(r)$ and $g_{D-Xe}(r)$ simulated in the mixture D_2O/xenon.

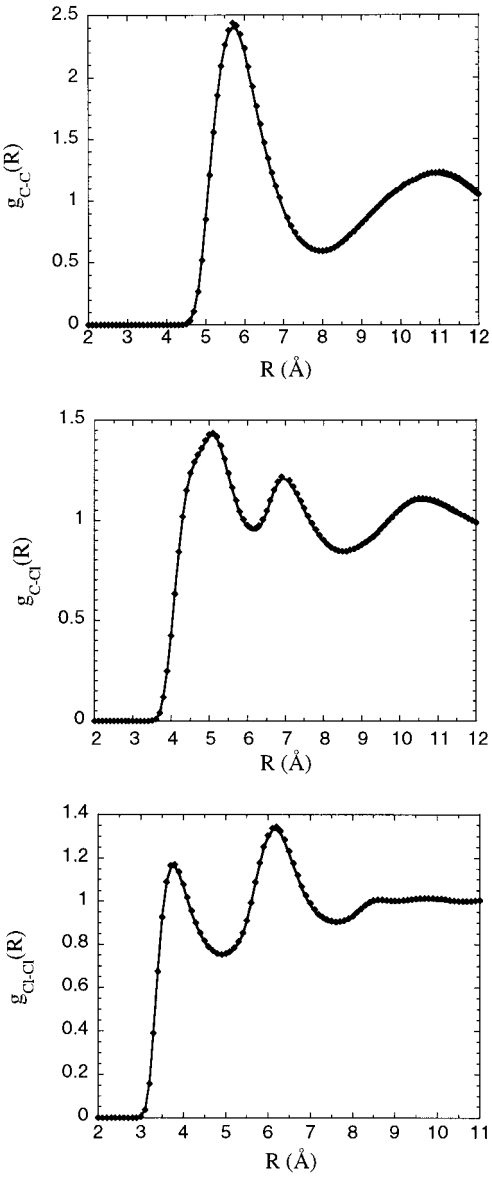

Figure 6. Comparison between the simulated rdf $g_{C-C}(r)$, $g_{C-Cl}(r)$, and $g_{Cl-Cl}(r)$ in the water/CCl_4 solution at room temperature (diamonds) with those calculated for the neat liquid CCl_4 (solid line) in the same thermodynamic conditions ($T \approx 300$ K and $\rho \approx 10.3 \times 10^{-3}$ mol/cm^3).

calculated in previous works.[49,52] The local ordering of water (H_2O and D_2O) diluted in liquid CCl_4 at room temperature and of D_2O dissolved in SC xenon fluid is now discussed from the analysis of the atom−atom pair distribution functions $g_{ij}(r)$.

D_2O in SC Xenon. For deuterated water dissolved in SC xenon, the atom−atom radial distribution functions (rdf) $g_{Xe-Xe}(r)$ calculated for the solution and for the pure SC fluid xenon are reported in Figure 5a. As expected, they exhibit the same behavior on the studied range of interatomic distances. Therefore, the local order between the xenon atoms does not appear to be affected by water dissolved in the SC fluid. In the first shell, each xenon atom is surrounded on average by 11 nearest neighbors. A translational local order between Xe atoms is clearly visible as three shells are observed and respectively found at interatomic distances about 4.5 Å, 8.5 Å, and 12.5 Å. The calculated Xe−O and Xe-D pair distribution functions $g_{O-Xe}(r)$ and $g_{D-Xe}(r)$ are illustrated in Figure 5b. The rdf $g_{O-Xe}(r)$ is characterized by a first peak centered around 3.8 Å (compared with the Lennard−Jones $\sigma_{O-Xe} \approx 3.63$ Å) followed by a minimum around 6 Å and a second peak culminating at 8 Å.. The first peak corresponds to the first solvation shell, in which the water molecule is surrounded on average by 11 nearest Xe atoms. Comparatively, the first peak of the rdf $g_{D-Xe}(r)$ is rather broad, and its maximum at about 4.4 Å (instead of 3.8 Å for $g_{O-Xe}(r)$) is preceded by a slight shoulder around 3.7 Å. Nevertheless, the first minimum and the second peak of $g_{D-Xe}(r)$ coincide nearly with the ones observed on the rdf $g_{O-Xe}(r)$ (i.e., about 6 Å and 8 Å). From these features, it is clear that the water molecule is particularly confined in its solvent cage in which the relative motions of the solute involve only small fluctuations of the O−Xe interatomic distance around its mean value (∼3.8 Å). In contrast, the fluctuations of the relative distances between the Xe and deuterated hydrogen atoms around the mean value (∼4.4 Å) are more significant. Hence, this suggests that the orientation of the solute molecule is randomly distributed in the solvent cage. Finally, the simulated structural properties of the D_2O/SC xenon mixture agree with

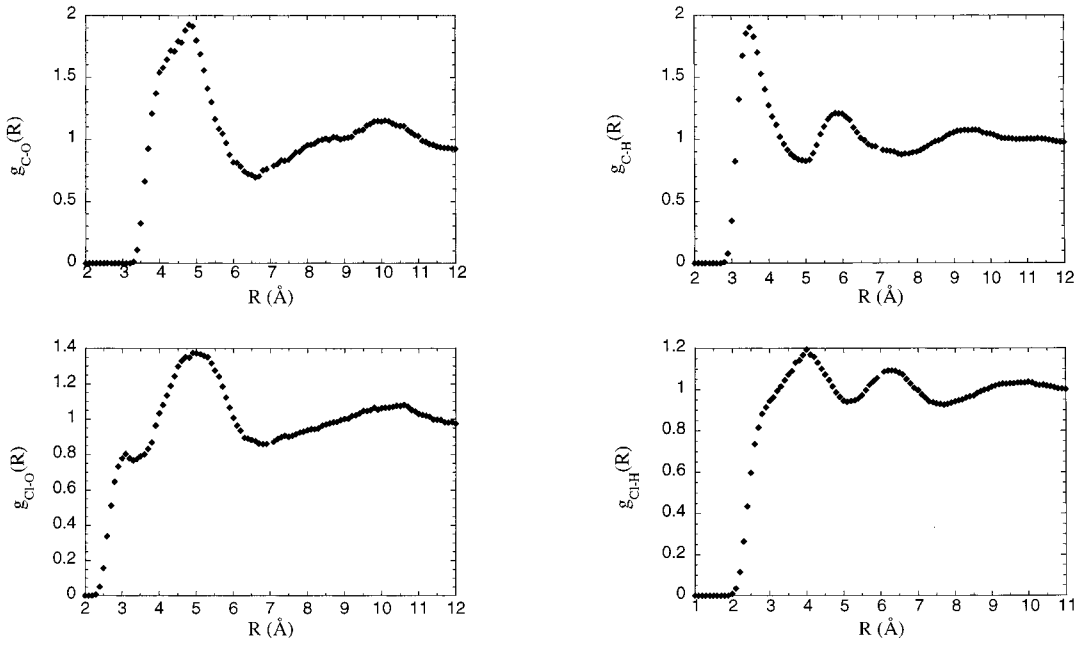

Figure 7. Atom−atom rdf $g_{O-C}(r)$, $g_{O-Cl}(r)$, $g_{H-C}(r)$ and $g_{H-Cl}(r)$ calculated between a pair of water and CCl_4 molecules for the water/CCl_4 solution ($T \approx 300$ K and $\rho \approx 10.3 \times 10^{-3}$ mol/cm^3).

the van der Waals nature of the interactions existing between D_2O and the Xe atoms.

Water in Liquid CCl_4. For the neat liquid CCl_4 ($T = 300$. K), the interatomic rdf $g_{C-C}(r)$, $g_{C-Cl}(r)$, and $g_{Cl-Cl}(r)$ calculated for a pair of molecules are shown in Figure 6. As expected, their main features are in rather good agreement with the previous studies of Mc Donald et al. and Kölmel et al.[48,52] From a general viewpoint, the analytic form of the intermolecular potential and the molecular charge distribution used in our simulation do not introduce drastic modifications on the local ordering between the CCl_4 molecules, and we notice that each is surrounded on average by 13 nearest neighbors.

We now consider the solution of hydrogenated (or deuterated) water very diluted in liquid CCl_4, and in particular, we find that the interatomic rdf $g_{C-C}(r)$, $g_{C-Cl}(r)$, and $g_{Cl-Cl}(r)$ between a pair of CCl_4 molecules (Figure 6) in solution are quasi indistinguishable from those of the pure liquid. However, a deeper examination of the $g_{C-C}(r)$and $g_{C-Cl}(r)$ rdf indicates a very slight increase of the height at radial distances close to the two first peaks and a very small shift (∼0.1 to 0.2 Å) of the second peak toward greater distances. This phenomenon, although relatively weak because the water solutions studied here are highly diluted, should be assigned to a small perturbation of the local order induced by a solvation process. In this context, the quantitative analysis that follows and based upon the calculated rdf $g_{O-C}(r)$, $g_{O-Cl}(r)$, $g_{H-C}(r)$, and $g_{H-Cl}(r)$ between a pair of water and CCl_4 molecules can provide more physical insight in order to precise the local order around the solute molecule in its solvent cage (Figure 7). The rdf $g_{O-C}(r)$ (which is almost identical to the intermolecular rdf $g_{cm}(r)$ of the center of mass between a pair of water and CCl_4 molecules) for the water/CCl_4 solution exhibits a broad peak centered at distances about 4.5−4.7 Å. The first minima are situated at about 6.4 Å, and we found that the water molecule is on average surrounded by 8 neighboring solvent molecules. The rdf $g_{O-Cl}(r)$ exhibits a broad peak centered at distances about 5 Å, leading to the same main conclusions as those provided from the rdf $g_{O-C}(r)$ (Figure 7). However, this peak is now broader because the chlorine atoms distribution around the oxygen of water is larger. However, a well-defined peak at about 3 Å is equally observed. This feature is assigned to the signature of a short-ranged O···Cl arrangements between water and CCl_4 molecule. Beyond distances of about 4 Å, the rdf $g_{O-Cl}(r)$ for the water diluted in liquid CCl_4 shows a third peak associated with the second shell at about 10 Å. Considering the rdf $g_{C-H}(r)$, a short-ranged local arrangement between the proton of water and the carbon atoms of CCl_4 is suggested by the well-defined sharp peak observed at about 3.5 Å. In the first shell (distances < 7.2 Å), the second peak clearly observed at distances of about 6 Å arises from the mean distance between the second hydrogen atom of water and the carbon atoms of the solvent molecules. Beyond distances of about 5.5 Å, the rdf $g_{C-H}(r)$ exhibits a peak at about 9.5 Å associated with the second shell of solvent molecules around water.

From these findings, the local ordering in these water/CCl_4 solutions can be discussed. First of all, the presence of a quasi-linear C···H−O arrangment with the C···O distance of about 4.5 Å is revealed from the position of the peak observed on $g_{C-H}(r)$ at 3.5 Å and $g_{C-O}(r)$ at 4.5 Å. In this situation, the expected interatomic O···Cl distances between the closest neighbors should be effectively at about 3.5 Å. Clearly, the existence of the first peak on $g_{O-Cl}(r)$ at about 3 Å requests the consideration another short-ranged arrangement between water and a second neighboring solvent molecule. For this purpose, a second O···Cl−C arrangement involving C···O interatomic distances of about 4.7 Å and corresponding to the position of the first peak observed on the rdf $g_{C-O}(r)$ needs to be considered. In this case, the Cl···H distances between closest neighbors are expected at about 4.Å. This conclusion is consistent with the observation of the first peak observed on $g_{Cl-H}(r)$ and the second peak observed at 5.7 Å on $g_{C-H}(r)$. Finally, the simulated structural properties of water in liquid CCl_4 reveal that a C···H−O short-ranged arrangement is favored between the solute and the surrounding solvent molecules. In this situation, one proton of water points toward the carbon atom of a CCl_4 molecule. This structural solute−solvent conformation presents some similarities with the calculated structure of the isolated H_2O-CCl_4 dimer,[53] although the mean interatomic distance O···C is found to be greater in our simulations. For the hydrogenated water solution, we found that this short-ranged

local order coexists on average with a secondary O···Cl−C short-ranged arrangement of water involving a second neighboring solvent molecule.

IV-3-B Rotational Dynamics of Monomeric Water in Hydrophobic Solvents. This section is aimed at a discussion of the influence of the water−solvent interactions on the reorientational dynamics of water. In particular, we investigate the contribution of the rotational relaxation mechanism in the broadening of the IR absorption profiles associated with the internal modes of water, which are governed by both rotational and vibrational processes.

From molecular dynamics simulations, the first insights concerning the rotational dynamics of the water molecule in its solvent cage are provided from the analysis of the individual time (classical) autocorrelation functions (acf) defined by

$$C_{u\xi}(t) = < u_\xi(t) \cdot u_\xi(0) > \quad (13)$$

which are associated with the unit vector u_ξ (ξ = x, y, z) lying along the corresponding main symmetry axes of the asymmetric rotor.

Nevertheless, for the sake comparison with the observed IR absorption profiles, it is convenient to analyze the simulated rotational spectral densities $G_{u\xi}(\omega)$. Because the simulation gives only access to the "classical" rotational spectral densities of water, the detailed balance conditions have been applied to desymmetrize the $G_{u\xi}(\omega)$ profiles (centered on the zero frequency).[54,55] Consequently, the latter profiles were obtained from the time Fourier transform of the corresponding simulated acf $C_{u\xi}$(t), i.e.,

$$G_{u\xi}(\omega) = \frac{1}{2}(1 + \exp(-\beta\hbar\omega))\frac{1}{2\pi}\int_{-\infty}^{+\infty} dt C_{u\xi}(t)e^{-i\omega t} \quad (14)$$

In the following, the rotational relaxation processes of water around its main symmetry axes have been quantitatively analyzed and comparatively discussed from the results obtained in supercritical xenon fluid, considered here as the reference system.

System D_2O/SC Xenon. We briefly summarize our main results obtained from MD simulation on the rotational dynamics of heavy water in the SC xenon fluid ($T \approx 383$ K and $\rho \approx 15.6 \times 10^{-3}$ mol/cm^3). First of all, the simulated acf $C_{u\xi}(t)$ of D_2O are reported in Figure 8. Notice that the small oscillations observed on the functions $C_{u\xi}(t)$ for times greater than 1 ps result from a residual statistical noise (the correlations are evaluated from only one heavy water molecule on a sampling time about 5 ps). The calculated correlation times associated with the reorientation of each axes of the heavy water in the SC xenon are given in Table 5. For comparison with the observed IR profiles, we analyze in detail the reorientational dynamics of D_2O from the simulated rotational profiles $G_{u\xi}(\omega)$ which are reported in Figure 9. Clearly, the spectral densities associated with the reorientational motions of the unit vectors u_x and u_y of D_2O exhibit a well-defined PQR type rotational band shape. The full widths at half-height $\Delta\nu$ of the central Q-branches associated with the C- and A- type rotational bands respectively at values of about 14 and 15 cm^{-1} (estimated with a relative uncertainties of about 10−15%). In contrast, the band shape of the simulated profile $G_{u_z}(\omega)$ relative to the reorientational motions of the C_2 symmetry axis u_z of D_2O is undoubtedly characterized by a rotational PR structure.

Clearly, the rotational band shapes obtained from the simulation indicates that the rotational motions of D_2O in SC xenon are almost unhindered. This conclusion arises from the comparison of the simulated profiles with those analytically calculated (using here the J-model with $\tau_J^* \sim 10$ vide supra) presented in Figure 9. Therefore, our results support the main

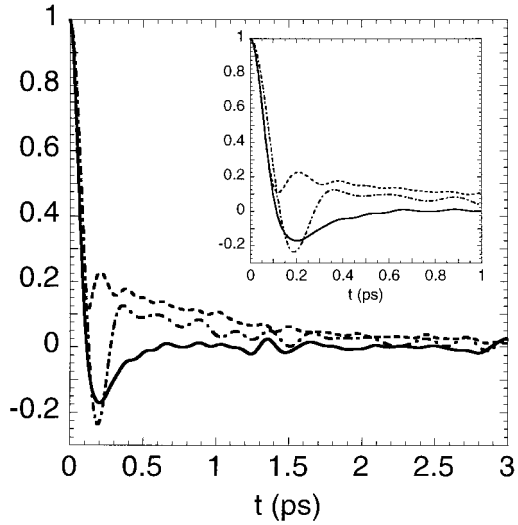

Figure 8. Simulated autocorrelation functions $C_{u\xi}(t)$ associated with the reorientational motions of the unit vectors $\boldsymbol{u}_x$ (dashed lines), $\boldsymbol{u}_y$ (point-dashed line-points) and $\boldsymbol{u}_z$ (solid line) lying along the main symmetry axes of D_2O in SC xenon. We have reported the same functions only up to 1ps in the inset.

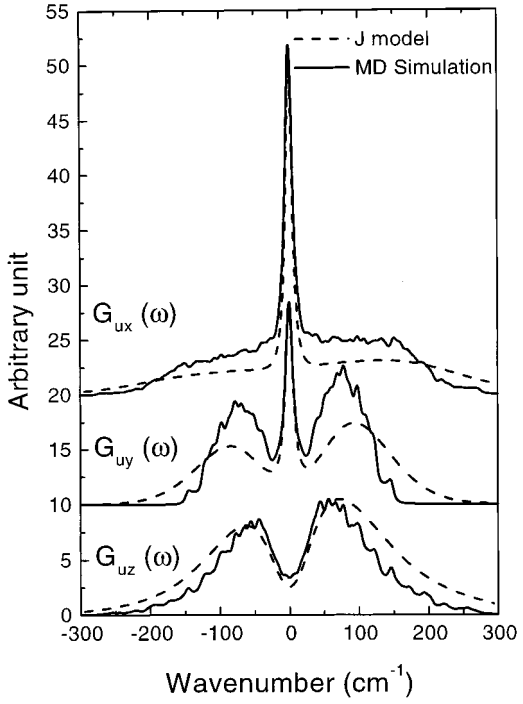

Figure 9. Rotational spectral densities $G_{u\xi}(\omega)$ associated with the reorientational motions of the unit vectors u_x (C-type band), u_y (A-type band), and u_z (B-type band) of D_2O in SC xenon from the simulation (solid lines) and calculated with $\tau^*_J \approx 10$ and $T = 383.15$ K using the J-model (dashed-lines).

TABLE 5: Calculated Correlation Times Associated with the Reorientational Motions of Each Axes of Water in Liquid CCl_4 ($T \approx 300$ K Density $\rho \approx 10.3 \times 10^{-3}$ mol/cm^3) and in SC Xenon Fluid ($T \approx 383$ K and $\rho \approx 15.6 \times 10^{-3}$ mol/cm^3)

	τ_{ux} (ps)	τ_{uy} (ps)	τ_{uz} (ps)
D_2O/SC xenon	0.28	0.16	0.24
D_2O/CCl_4	0.22	0.29	0.43
H_2O/CCl_4	0.28	0.51	0.50

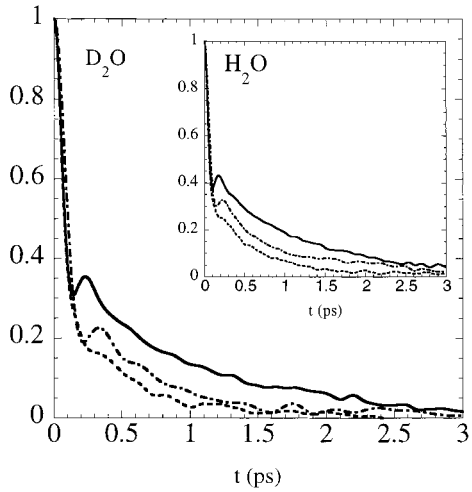

Figure 10. Simulated autocorrelation functions $C_{u\xi}(t)$ associated with the unit vectors $\boldsymbol{u}_x$ (dashed lines), $\boldsymbol{u}_y$ (point-dashed line-points), and $\boldsymbol{u}_z$ (solid line) for D_2O diluted in liquid CCl_4 at room temperature (and for H_2O in liquid CCl_4 in the inset).

conclusions arising from the previous study of Bowman et al.[12] concerning the predominant importance of the rotational process in conditioning the shape of the ν_3 profile. Nevertheless, the role of the ν_1 mode contribution in the spectral range situated at about 2700 cm^{-1} for D_2O as been left hanging. For this purpose, we have compared the experimental spectrum measured by these authors with the spectrum calculated as a weighted sum of the simulated type A (for the ν_1 mode) and type B (for the ν_3 mode) profiles. This comparison is displayed in Figure 1 and shows that it is only possible to obtain a rather good agreement with the weighting coefficients having the respective values of about 0.4 (for the ν_1 mode) and 1.2 (for the ν_3 mode). We notice that the ratio of the integrated intensities of the ν_1 profile by the ν_3 one is about 1/3, a value which is much greater than the one obtained for water in gas phase ($\sim$1/15).[14] Although the main conclusions concerning the ν_3 profile raised by Bowman et al. are still valid, we also find that the ν_1 mode contribution in the resulting profile is not negligible. This result is perhaps the clue to understand the fact observed but not discussed, that the P wing seems apparently more intense than the R wing on the IR experimental spectrum. Indeed, if the IR spectrum was only due to the ν_3 transition, we should expect according to the detailed balance that the P wing is less intense than the R one. Finally, it appears that the vibrational processes involved in both the ν_1 and ν_3 modes of water contribute only very slightly in the broadening mechanism of the band shapes. However, the enhancement of the intensity of the ν_1 mode is related to the increasing of the corresponding dipole transition $\partial\mu/\partial q_1$ due to the van der Waals nature of the interactions applied on the water molecule in its solvent cage.

System Water/CCl_4. As before, we will put the emphasis in this section on the band shape analysis of the spectral densities in order to assess the reorientational dynamics of water. However, we briefly comment on the main features obtained in the time domain. For this purpose, we have displayed in Figure 10 the simulated time acf $C_{u\xi}(t)$ (ξ = x, y, z) and reported in Table 5 the corresponding correlation times for D_2O and H_2O. Clearly, the overall time behavior of the simulated acf $C_{u\xi}(t)$ are rather different than those found in SC xenon (compare Figure 8 and Figure 10). Indeed, they are characterized by a decrease taking place on two well-separated time scales. At short times (t < 0.15 ps), the acf $C_{u\xi}(t)$ are rapidly decreasing. This indicates that the water molecule is not affected by interactions with the solvent molecules and rotates freely (it is the so-called

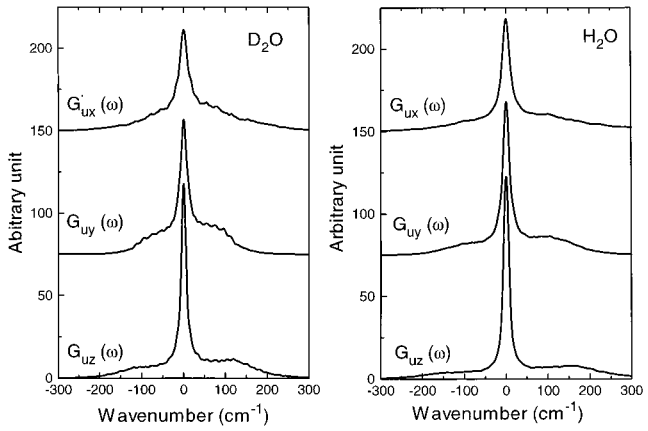

Figure 11. Simulated rotational spectral densities $G_{u\xi}(\omega)$ associated with the reorientational motions of the distinct x, y, and z symmetry axes of D_2O and H_2O dissolved in liquid CCl_4.

inertial regime). At longer times (t > 0.3ps), all of these relaxation functions are characterized by a tail that slowly decreases and shows that the rotational diffusive regime of water is reached. Therefore, deviations from the "free" rotational dynamics of water is observed on all the acf $C_{u\xi}(t)$. In particular, we notice that the reorientational motions of the C_2 symmetry axis of water appears the most affected by the interactions with the solvent molecules $C_{u_z}(t)$ (Figure 10). Therefore, it can be presently inferred from this preliminary analysis in the temporal domain that the rotational bands should differ appreciably from those corresponding to the free rotation limit. For this purpose, we will thoroughly analyze the simulated spectral densities $G_{u\xi}(\omega)$ (ξ = x, y, z) reported in Figure 11. For D_2O, the spectral density $G_{u_x}(\omega)$ due to the reorientational motions of the unit vector u_x out of the molecular plane of water (type C band) exhibits an intense central peak having very broad wings which are reminiscent of the free rotational wings. The value of the full width at half-height $\Delta\nu_C$ of the central peak is at about 26 cm^{-1}. The spectral density $G_{u_y}(\omega)$ associated with the reorientational dynamics of the unit vector u_y of heavy water (type A band) presents a central branch characterized by a full width at half-height $\Delta\nu_A \approx 23$ cm^{-1}. This peak is flanked with well-defined wings, suggesting that the rotational motions of the *y*-axis of water is less hindered than the one of the *x* axis. Finally, the profile $G_{u_z}(\omega)$ due to the reorientational motions of the C_2-symmetry axis of water (type B band), exhibits an intense central peak accompanied on both sides with very weak wings. Clearly, the appearance of the central branch on this simulated profile indicates strongly perturbed reorientational motions of the C_2-symmetry axis. The full width at half-height $\Delta\nu_B$ of the central branch has a value of about 14 cm^{-1} is due to the relaxation process of the unit vector u_z, which is due to the rotational diffusion mechanism at the long time in liquid CCl_4. This diffusive phenomenon also plays a role in the long-time part of the reorientational relaxation processes of the unit vectors u_x and u_y of D_2O (shown in Figure 10) and governs the broadening mechanism of the corresponding central branches of the simulated rotational profiles $G_{u\xi}(\omega)$ (ξ = x, y, z).

The same conclusions can be reached from the band shape analysis of the rotational bands calculated for light water diluted in liquid CCl_4 (Figure 11). As expected, due to the smaller values of the inertial moment of H_2O, the main spectral deviations observed this time on the rotational profiles, $G_{u_x}(\omega)$ and $G_{u_y}(\omega)$, are the frequency positions of the maxima of the envelop of the rotational wings. Furthermore, the widths of the central branches are narrower and have the respective values of about $\Delta\nu_C \approx 23$ cm^{-1} and $\Delta\nu_A \approx 20$ cm^{-1} (instead of 26

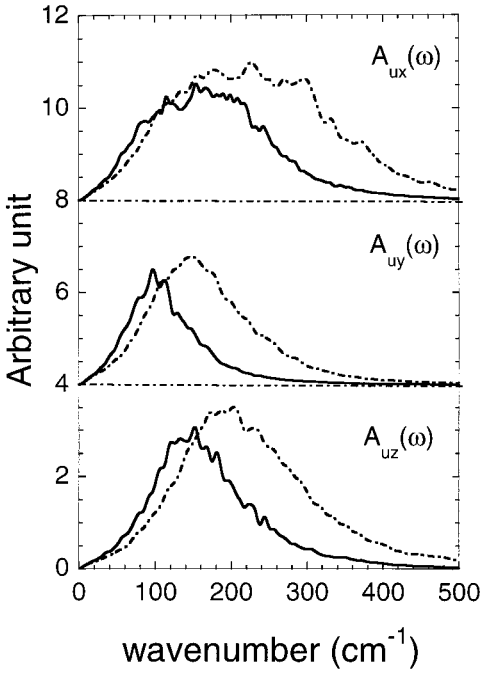

Figure 12. Simulated power spectra $A_{u_\xi}(\omega)$ associated with reorientational motions of the distinct x, y, and z symmetry axes of D_2O (solid lines) and H_2O (dashed-lines) in liquid CCl_4.

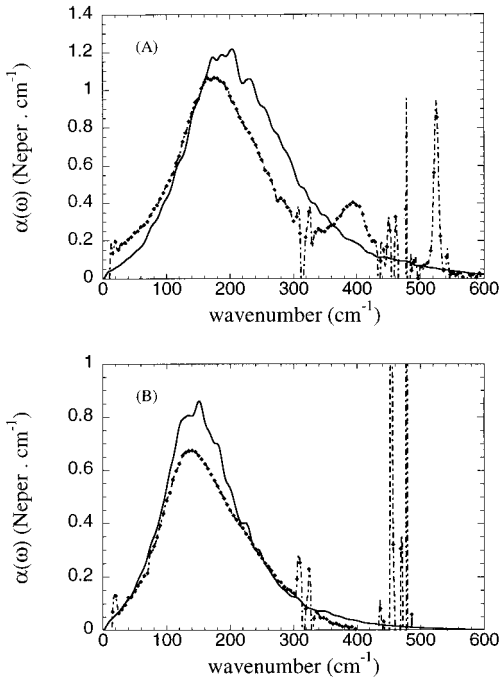

Figure 13. Comparison of the simulated far-IR profiles of H_2O (A) and D_2O (B) dissolved in liquid CCl_4 (solid lines) with the corresponding experimental spectra (dashed-lines).

cm^{-1} and 23 cm^{-1} for heavy water). Compared with the free rotation, the band shape of the rotational profile $G_{u_z}(\omega)$ is also found strongly modified in liquid CCl_4, as indicated by the appearance of a narrow central peak for H_2O ($\Delta\nu_B \approx 14$ cm^{-1}).

From these findings, it can be inferred that the reorientational dynamics of water (H_2O and D_2O) in liquid CCl_4 at room temperature is singularly affected by the solute−solvent interactions. Indeed, the surprising appearance of the central peak on the simulated spectral density $G_{u_z}(\omega)$ reveals a reorientation dynamics of the C_2-symmetry axis of water strongly affected at long-times ($t > 0.3$ps), which is governed by diffusive relaxation processes although remnant rotational wings are still observed at much shorter times. Therefore, the reorientational motions associated with the main symmetry axes of water appears to be differently affected by the interactions with the neighboring solvent molecules.

Indeed, we found that the reorientational dynamics of the *y* axis are nearly free, whereas the reorientational motions of the *z* symmetry axis of water are strongly hindered. Incidentally, let us emphasize that the J model is unable to lead for a type B band composed of an intense central peak accompanied with residual rotational wings as obtained in the simulation. Clearly, the short-time reorientational dynamics of water probed through these rotational wings (∼150−300 fs) primarily depends of the nature of the intermolecular interactions of the solute with the neighboring molecules.

At this stage of our study, it is interesting to further analyze the rotational wings in order to get more physical insight about the faster reorientational relaxation processes of water taking place in liquid CCl_4. For this purpose, we have calculated the power spectra $A_{u_\xi}(\omega)$ ($\sim\omega(1 - e^{-\beta\hbar\omega})G_{u_\xi}(\omega)$, with ξ = x, y, z) associated with the reorientational motions of the different molecular axes of water in its solvent cage (Figure 12). As shown in Figure 12, the band shape of the spectrum associated with the reorientational motions of the unit vector u_y of H_2O (and D_2O) is characterized by a broad band that peaks at a frequency value of approximately 150 cm^{-1} (respectively 100 cm^{-1} for D_2O). The power spectrum associated with the reorientational motions of the C_2-symmetry axis of H_2O (and D_2O) (cf. Figure 12) exhibits a broad profile centered at a frequency value of about 190 cm^{-1} (correspondingly 150 cm^{-1} for D_2O). In this context, it is particularly interesting to compare the simulated far-IR profiles of water (H_2O and D_2O) dissolved in liquid CCl_4 with the experimental ones (see figures 13A and 13B).[15] For this purpose, we have considered the profiles as primarily governed by the dipole relaxation process of a solitary water molecule in its solvent cage. In other terms, the simulated profiles shown in Figure 13 have been simply obtained in a first approximation by the relationship (without induced dipole interaction processes)

$$\alpha^{(FIR)}(\omega) = c_S \mu_w^2 A_{u_\xi}(\omega) \qquad (15)$$

where c_s is the solubility (in mol l^{-1}) of water in liquid CCl_4 (respectively of about 8.9×10^{-3} M and 7.4×10^{-3} M for H_2O and D_2O at room temperature),[44] and μ_w is the permanent dipole moment of water (taken here at the value of 1.9 D).

We observe that the band shapes of the simulated far-IR absorption profiles are in fair agreement with those measured and exhibit broad bands centered at about 190 and 150 cm^{-1} for H_2O and D_2O, respectively (see Figures 13A and 13B). A further analysis, which is not discussed here, clearly shows that the agreement between the simulated and measured far-infrared (FIR) absorption spectra of water in liquid CCl_4 can be improved by explicitly taking into account the interaction-induced dipoles mechanisms in these solutions. Although it represents a minor contribution, the role played by the interaction-induced absorption processes on the far-IR profiles of water in such hydrophobic solvents constitutes a relevant key point of our study that merits some additional comments, which will be addressed in a forthcoming paper.[56]

V Discussion

A physical insight on the vibrational relaxation contribution in each of the ν_1 and ν_3 stretching modes of water diluted in

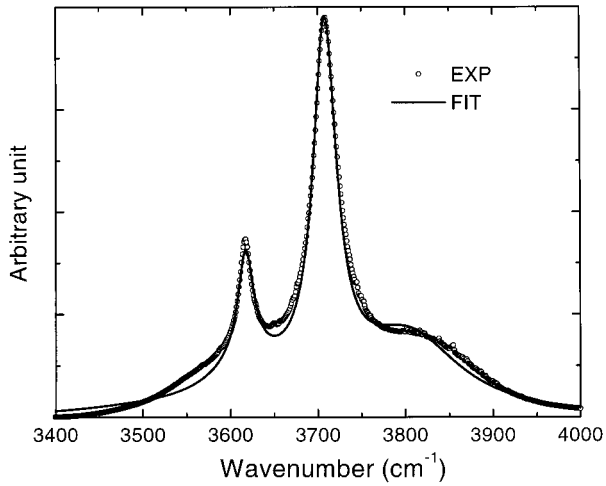

Figure 14. Comparison of the infrared spectrum of H_2O diluted in liquid CCl_4 (filled circles) with the calculated profile (solid line) obtained from the convolution according to the eq 14 of the simulated rotational spectral densities associated with the *z* axis (for the ν_1 mode) and the *y* axis (for the ν_3 mode) of solute with the adjusted vibrational profiles (assumed of type Lorentzian).

liquid CCl_4 can be obtained from the comparison of the experimental spectrum with the profile calculated according to the following treatment. The simulated spectral densities associated with the reorientational motions of the *z* axis (for the ν_1 mode) and the *y* axis (for the ν_3 mode) have been respectively convoluted by Lorentzian profiles in order to take into account the vibrational relaxation contribution associated with each of the corresponding modes. The calculated spectrum is obtained from a weighted sum of the two previous profiles according to the following expression

$$\alpha^{(calc)}(\omega) = \frac{4\pi^2}{3\hbar cV}\omega(1 - \exp(-\beta\hbar\omega))\{\eta_1 G_z^{(rot)}(\omega)\otimes L_{V_1}^{vib}(\omega - \omega_1) + \eta_3 G_y^{(rot)}(\omega)\otimes L_{\nu_3}^{vib}(\omega - \omega_3)\} \quad (15)$$

where η_1 and η_2 are the weighting coefficients, and $L_{\nu i}^{vib}(\omega - \omega_i)$ is the vibrational Lorentzian profile centered at the angular frequency ω_i.

In this treatment, the vibrational full widths and the weighting coefficients are taken as adjustable parameters. The comparison of the calculated spectrum with the experimental one is displayed in Figure 14. This good agreement is obtained using vibrational full widths having respective values $\Delta_{\nu_1}^{vib} \approx 7.5$ cm^{-1} and $\Delta_{\nu_3}^{vib} \approx 12$ cm^{-1} and a ratio $\eta_1/\eta_3 \approx 3.5$. Clearly, this result shows that the IR profiles cannot be interpreted on the basis of the rotational contribution alone and that the vibrational relaxation processes must be taken into account in the broadening mechanism of both ν_1 and ν_3 band shapes. Moreover, it also comes out from this quantitative analysis that the ν_1 vibrational mode of water in liquid CCl_4 is more affected by the solute−solvent interactions as indicated by the enhancement of its intensity. Indeed, the oscillator strength of the fundamental ν_1 vibrational transition of water is increased by a factor 3.8 on going from the gaseous phase to liquid CCl_4. In contrast, the oscillator strength value of the fundamental ν_3 transition remains very close to its gas-phase value (cf. discussion in section III-2 and Table 1).

VI Conclusion

In this paper, we have shown that the infrared spectroscopy is particularly well-adapted to probe the interactions of water with hydrophobic solvents on a picosecond time-scale. For the most "inert" solvent like xenon, we found that the rotational relaxation processes play a predominant role in controlling the shape of the IR absorption profiles associated with the ν_1 and ν_3 stretching modes and that the vibrational relaxation contributions can safely be neglected. In particular, in these solvents, the water molecule is found to rotate almost "freely" around all its main molecular axes, a fact that is ascribed to the isotropic character of the van der Waals interactions applied on the solute. Moreover, the transition dipole moment of the ν_3 mode of water is only weakly affected by the interactions with the Xe atoms and remains nearly at its gas-phase value. In contrast, it appears that the oscillator strength of the ν_1 internal mode is increased. Hence, suggesting that this last vibration is more sensitive to the intermolecular interactions. In this context, the use of molecular dynamics simulations to treat the purely rotational contribution of the spectra associated with the ν_3 and ν_1 vibrational modes of water is convenient and of great interest. Furthermore, it was shown that the analytical treatment based upon Gordon's J-model for asymmetric-molecular rotors provides valuable insight on the rotational dynamics of water primarily governed by collisional interactions with the neighboring solvent molecules.

For water dissolved in liquid CCl_4, the existence of an octopole−dipole electrostatic contribution between the interacting partners has consequences on both the structural and the dynamical properties. In the former case, our study has demonstrated the existence of a short-ranged C···H−O structure between the solute and its neighboring solvent molecules. Furthermore, such weak solute−solvent interactions have more sizable effects on the reorientational dynamics of water in liquid CCl_4 than in SC xenon fluid. Indeed, it is found that the mean intermolecular torque applied on the water molecule by its solvent cage affects differently the reorientational dynamics associated with each main symmetry axes of the solute. In particular, the reorientational motions of the z symmetry axis of water appears more specifically affected by the solute−solvent interactions as revealed by the band shape analysis of the ν_1 infrared absorption profile. In conclusion, the main difference observed on the rotational dynamics of water in liquid CCl_4 must be ascribed to the weakly anisotropic character of the solute−solvent interactions of electrostatic nature. Clearly, the rotational relaxation processes of water depend on a detailed description of the potential applied on the solute by the surrounding solvent molecules. In this context, we must emphasize that the correct treatment of the classical rotational dynamics of water (H_2O or D_2O) in liquid CCl_4 may only be provided up to now by simulation studies and that the use of currently available analytical approaches (J-model, for instance) need to explicitly include the details of the solute−solvent potential. Another important viewpoint concerning the statement about the existence of a very weak H-bond complex between water and CCl_4 molecules also merits emphasizing.[11] Clearly, we have been able to interpret the spectral properties by taking into account only the electrostatic forces without invoking a specific H-bond contribution in the intermolecular potential.

When compared with the study of water in xenon, the contribution of the vibrational processes in the IR absorption profiles now plays a significant role in the band shapes, the intensity enhancements, and the frequency shifts of the stretching modes of water. The vibrational relaxation processes contribute to 40% and 30% of the total broadening observed on the profiles associated with the ν_1 and ν_3 internal modes of water, respectively. Moreover, the intensity of the ν_1 internal mode is

found to be about four times greater than that found for water in gaseous phase. In contrast, within experimental uncertainties, the intensity of the ν_3 internal mode remains fairly close to its gas phase value. Finally, the vibrational frequencies are found red-shifted from their gas phase values, a fact consistent with the existence of attractive forces between the two partners. Adopting the early terminology used in the literature, we may conclude that the liquid CCl_4 can be considered as a "more interacting" solvent than xenon. From our study, this implies that the interaction with the solvent leads to hindered rotational motions of water with a greater anisotropic character, whereas the vibrational processes play an increasingly role on the infrared spectra. Therefore, it should be inferred that the former contribution is vanishingly small for water dissolved in more interacting solvent. Thus, upon increasing the strength of the interaction between water and the solvent, it is necessary to explicitly consider the vibrational relaxation mechanism of the internal modes of water with the solvent molecules in an exhaustive approach aimed at performing a quantitative analysis of the mid-infrared absorption spectra.

Acknowledgment. The authors are pleased to thank Dr Y. Guissani and Dr. J. -Cl. Leicknam (L.P.T.L. CNRS (UMR 7600), Université Paris VI) for kindly providing the computer program concerning the J-model of asymmetric top molecules and also for helpful discussions. We especially acknowledge Dr B. Guillot for his valuable comments and for critically reading this manuscript. The help of Mr L. Lagardère in collecting part of the experimental data has been appreciated. We acknowledge the computer center IDRIS of the CNRS (Institut du Développement et des ressources en Informatique Scientifique, Orsay) and the MASTER of the ENSPCB (Université de Bordeaux I) for allocating computing time and providing facilities.

References and Notes

(1) Errera, J. *J. Chimie Physique* **1937**, *34*, 617.
(2) Borst, L. B.; Buswell, A. M.; Rodebush, W. H. *J. Chem. Phys.* **1938**, *6*, 61.
(3) Fox, J. J.; Martin, A. E. *Proc. R. Soc.* **1940**, *74A*, 234. Greinacher, E.; Lüttke, W.; Mecke, R. *Ber. Bunsen-Ges. Phys. Chem.* **1955**, *59*, 23.
(4) Saumagne, P.; Josien, M. L. *Bull. Soc. Chim. Fr.* **1958**, 813.
(5) Saumagne, P. Ph.D. Thesis, Bordeaux, 1961.
(6) Le Narvor, A.; Gentric, E.; Saumagne, P. *Can. J. Chem.* **1971**, *49*, 1933. Le Narvor, A.; Gentric, E.; Saumagne, P. *J. Chem. Soc., Faraday Trans. 2* **1974**, *70*, 1191.
(7) Glew, D. N.; Rath, N. S. *Can. J. Chem.* **1971**, *49*, 837.
(8) Burneau, A.; Corset, J. *J. Chimie Physique* **1972**, *1*, 142.
(9) For example, see: HITRAN Database Rothman, L. S.; Gamache, R. R.; Tipping, R. H.; Rinsland, C. P.; Smith, M. A. H.; Benner, D. C.; Divi, V. M.; Thand, J. M.; Camy-Peyret, C.; Perrin, A.; Goldman, A.; Massie, S. T.; Brown, L. R.; Toth, R. A.; *J. Quant. Spectrosc. Radiat. Transfer* **1992**, *48*, 469 (and references therein).
(10) Conrad, M. P.; Strauss, H. L. *Biophys. J.* **1985**, *48*, 117.
(11) Conrad, M. P.; Strauss, H. L. *J. Phys. Chem.* **1987**, *91*, 1668.
(12) Bowman, L. E.; Palmer, B. J.; Garrett, B. C.; Fulton, J. L.; Yonker, C. R.; Pfund, D. M.; Wallen, S. L. *J. Phys. Chem.* **1996**, *100*, 18 327.
(13) Burneau, A. Ph.D. Thesis, Paris, 1970. Burneau, A. *J. Mol. Liq* **1990**, *46*, 99.
(14) Kjaergaard, H. G.; Henry, B. R.; Wei, H.; Lefebvre, S.; Carrington, T., Jr.; Mortensen, O. S.; Sage, M. L. *J. Chem. Phys.* **1994**, *100*, 6228.
(15) Tassaing, T.; Danten, Y.; Besnard, M.; Zoidis, E.; Yarwood, J.; Guissani, Y.; Guillot, B. *Mol. Phys.* **1995**, *84*, 769, and references therein.
(16) Zoidis, E.; Yarwood, J.; Tassaing, T.; Danten, Y.; Besnard, M. *J. Mol. Liq.* **1995**, *64*, 197.
(17) Suzuki, S.; Green, P. G.; Bumgarner, R. E.; Dasgupta, S.; Goddard, W. A., III; Blake, G. A. *Science* **1992**, *257*, 942.
(18) Klemperer, W. *Nature* **1993**, *362*, 698.
(19) Kim, K. S.; Lee, J. Y.; Choi, H. S.; Kim, J.; Yang, J. H. *Chem. Phys. Lett.* **1997**, *265*, 497.
(20) Gregory, J. K.; Clary, D. C. *Mol. Phys.* **1996**, *88*, 33.
(21) Augspurger, J. D.; Dykstra, C. E.; Zwier, T. S. *J. Phys. Chem.* **1992**, *96*, 7252.
(22) Karlström, G.; Linse, P.; Wallqvist, A. Jönsson, B. *J. Am. Chem. Soc.* **1983**, *105*, 3777.
(23) Engdahl, A.; Nelander, B. *J. Chem. Phys.* **1985**, *89*, 2860.
(24) Engdahl, A.; Nelander, B. *J. Chem. Phys.* **1987**, *91*, 2860.
(25) Gutowsky, H. S.; Emilsson, T.; Arunan, E. *J. Chem. Phys.* **1993**, *99*, 4883.
(26) Gotch, A. J.; Zwier, T. S. *J. Chem. Phys.* **1992**, *96*, 3388.
(27) Pribble, R. N.; Zwier, T. S. *Science* **1994**, *265*, 75.
(28) Pribble, R. N.; Zwier, T. S. *Faraday Discuss.* **1994**, *97*, 229.
(29) Pribble, R. N.; Garrett, A. W.; Haber, K.; Zwier, T. S. *J. Chem. Phys.* **1995**, *103*, 131.
(30) Furatcha, S.; Ikawa, S. *J. Chem. Phys.* **1998**, *108*, 5159.
(31) Furatcha, S.; Ikawa, S. *J. Chem. Phys.* **1998**, *108*, 1347.
(32) Wakai, C.; Nakahara, M. *J. Chem. Phys.* **1995**, *103*, 2025.
(33) Nakahara, M.; Wakai, C. *J. Chem. Phys.* **1992**, *97*, 4413.
(34) Wakai, C.; Nakahara, M. *J. Chem. Phys.* **1997**, *106*, 7512.
(35) Tassaing, T.; Danten, Y.; Besnard, M.; Zoidis, E.; Yarwood, J. *Chem. Phys.* **1994**, *184*, 225.
(36) Besnard, M. In *Molecular Liquids: New perspectives in Physics and Chemistry*; NATO ASI Series C, **1992**, *379*, 513.
(37) Besnard, M.; Danten, Y.; Tassaing, T. *J. Chem. Phys.* **2000**, *113*, 3741.
(38) Tassaing, T. *Vibrat. Spectrosc*., to be published.
(39) Danten, Y.; Tassaing, T.; Besnard, M. *J. Phys. Chem.* **1999**, *103*, 3350.
(40) Gordon, R. G. *J. Chem. Phys.* **1965**, *43*, 1307.
(41) Bratos, S.; Rios, J.; Guissani, Y. *J. Chem. Phys.* **1970**, *52*, 439.
(42) Besnard, M.; Lassègues, J. C.; Guissani, Y.; Leicknam, J. C. *Mol. Phys.* **1984**, *53*, 1145.
(43) Schofield, P. *Phys. Rev. Lett*. **1960**, *4*, 239.
(44) Goldman, S.; *Can. J. Chem.* **1974**, *52*, 1668. Backx, P.; Goldman, S. *J. Phys. Chem.* **1981**, *85*, 2975.
(45) Guissani, Y.; Leicknam, J. C.; Bratos, S. *Phys. Rev. A* **1977**, *16*, 2072.
(46) Aguado-Gomez, M.; Leicknam, J. C. *Phys. Rev. A* **1986**, *34*, 4195.
(47) Haase, J.; Zeil, W. *Z. Phys. Chem.* **1965**, *45*, 202.
(48) Ewool, K. M.; Strauss, H. L. *J. Chem. Phys.* **1973**, *58*, 5835.
(49) Mc Donald, I. R.; Bounds, D. G.; Klein, M. L. *Mol. Phys.* **1982**, *45*, 521.
(50) Berendsen, H. J. C.; Postma, J. P. M.; van Gunsteren, W. F.; Hermans, J. In *Intermolecular Forces*; Pullmann, B.; Ed.; Dordrecht, 1981; 331.
(51) Mc Donald, I. R.; Singer, K. *Mol. Phys.* **1972**, *23*, 29.
(52) Kölmel, C.; Ahlrichs, R.; Karch, B. *Mol. Phys.* **1989**, *66*, 1015.
(53) Chang, T. M.; Dang, L. X. *J. Chem. Phys.* **1996**, *104*, 6772.
(54) Poll, J. D. *Intermolecular Spectroscopy and Dynamical Properties of Dense Systems*; van Kranendonk, J., Ed.; North-Holland, 1980.
(55) Borysow, J.; Frommhold, L. *Phenomena Induced by Intermolecular Interactions*; Birnbaum, G., Ed.; Plenum Press: 1985; p 67.
(56) Danten, Y.; Tassaing, T.; Besnard, M., in preparation